Available online at www.sciencedirect.com
ScienceDirect
Advances in Space Research 44 (2009) 46–53
ADVANCES IN SPACE RESEARCH (a COSPAR publication)
www.elsevier.com/locate/asr

Analyses of magnetic field structures for active region 10720 using a data-driven 3D MHD model

S.T. Wu [a,b,*], A.H. Wang [a], G. Allen Gary [a], Ales Kucera [c], Jan Rybak [c], Yang Liu [d], Bojan Vrśnak [e], Vasyl Yurchyshyn [f]

[a] Center for Space Plasma & Aeronomic Research, The University of Alabama in Huntsville, 301 Sparkman Drive, Huntsville, AL 35899, USA
[b] Department of Mechanical & Aerospace Engineering, The University of Alabama in Huntsville, 301 Sparkman Drive, Huntsville, AL 35899, USA
[c] Astronomical Institute, Slovak Academy of Sciences, 05960, Tatranska Lomnica, Slovakia
[d] W.W. Hansen Experimental Physics Laboratory, Stanford University, Stanford, CA 94305, USA
[e] Hvar Observatory, Faculty of Geodesy, Kačičeva 26, HR-10000 Zagreb, Croatia
[f] Big Bear Solar Observatory (BBSO) of New Jersey Institute of Technology (NJIT) 40386 North Shore Lane, Big Bear City, CA 92314, USA

Received 18 November 2008; received in revised form 3 March 2009; accepted 25 March 2009

Abstract

In order to understand solar eruptive events (flares and CMEs) we need to investigate the changes at the solar surface. Thus, we use a data-driven, three-dimensional magnetohydrodynamic (MHD) model to analyze a flare and coronal mass ejection productive active region, AR 10720 on January 15, 2005. The measured magnetic field from Big Bear Solar Observatory (BBSO) digital vector magnetograph (DGVM) was used to model the non-potential coronal magnetic field changes and the evolution of electric current before and after the event occurred. The numerical results include the change of magnetic flux (Φ), the net electric current (I_N), the length of magnetic shear of the main neutral line (L_{ss}), the flux normalized measure of the field twist ($\alpha = \frac{\mu I_N}{\Phi}$) with μ being the magnetic permeability. The current helicity (H_c) injected into the corona and the photospheric surface velocity are also computed. The characteristic parameters of the buildup process before the event and the decay process after the event are investigated and the amount of magnetic energy converted to drive the event is estimated.

Keywords: Sun-MHD; Photosphere – MHD; Non-potentiality properties – MHD; Sun – Magnetograms

1. Introduction

Flares and coronal mass ejections (CMEs) are spectacular phenomena which are usually associated with solar active region. Flares are considered as a local scale phenomena and CMEs have large, global scale; both phenomena expel mass, magnetic flux, and helicity through the corona into the interplanetary medium. The amount of mass expelled from the CME event is spectacularly large, on the order of 10^{15} g. The magnetic field and plasma in the ejected structure, combined with its momentum, can significantly disrupt the Earth's magnetospheric configuration, thereby exposing satellites to conditions outside the magnetosphere. Without this protective envelope the satellites are subject to failure. The flare's effect is more direct and faster via its associated solar energetic particle (SEP) events, which can also cause satellite failure. Thus, in order to give the longest advance warning to protect space facilities, it is imperative to enhance the current prediction capability for solar eruptive events to the magnetic pre-

* Corresponding author. Address: Center for Space Plasma & Aeronomic Research, The University of AL in Huntsville, 301 Sparkman Drive, Huntsville, AL 35899, USA.
E-mail addresses: wus@cspar.uah.edu (S.T. Wu), wanga@cspar.uah.edu (A.H. Wang), allen.gary@nasa.gov (G.A. Gary), akucera@ta3.sk (A. Kucera), choc@ta3.sk (J. Rybak), yliu@solar2.stanford.edu (Y. Liu), bvrsnak@geof.hr (B. Vrśnak), vayur@bbso.njit.edu (V. Yurchyshyn).

0273-1177/$36.00 © 2009 COSPAR. Published by Elsevier Ltd. All rights reserved.
doi:10.1016/j.asr.2009.03.020

eruption. Hence, we need to investigate magnetic changes on the solar surface. It is generally believed that the magnetic energy and helicity are brought into the corona as the emergence of the magnetic flux from the sub-photosphere. The magnetic energy release in solar active phenomena, such as flares and CMES, is provided by the non-potentional components of the magnetic field in active regions; whereby the quantification of the active region evolution becomes the first step to understand the developmental processes of the solar eruptive events such as flares and CMEs. Following Liu and Zhang's (2007) observational investigation of the relationship between the electric field and flares for this region (AR 10720) at January 17, 2005, we have focused on the CME that occur on January 15, 2005. A series of magnetograms provided our model with enough knowledge for us to model conditions for the initiation of the CME. We employ the recently developed data-driven 3D magnetohydrodynamic (MHD) model to analyze the January 15, 2005 NOAA/AR 10720 for the quantification of the non-potentiality parameters to understand the physical characteristic of AR 10720. Our focus was on the conditions of pre- and post-CME.

The non-potentiality parameters investigated include the magnetic shear, total magnetic flux, net current, and the field twist as introduced by Falconer et al. (2002). Other important physical quantities such as the current helicity and transverse velocity resulting from the photospheric dynamo were examined. Similar types of investigations have been performed by many investigators (Chae, 2001; Chae et al., 2004; Deng et al., 2001; Demoulin et al., 2002; Kusano et al., 2002; Moon et al., 2002; Nindos et al., 2003; Nindos and Andrews, 2004; Liu and Zhang, 2006, 2007). Most notably, Liu and Zhang (2007) investigated the relationship between inductive electric field and flares based on AR 10720, 10486, 9077 and 8100. Demoulin et al. (2002), Kusano et al. (2002), Moon et al. (2002) and Nindos et al. (2003) have performed a study of the magnetic helicity budget of solar active region and coronal mass ejections using either potential field model or linear force-free field model. But, all these studies did not use a self-consistent magnetohydrodynamic model. It is critical to account for the interactions between the plasma motion and magnetic field to determine the physical properties to understand the eruption physics.

A brief description of the observation during the period of the CME is given in Section 2, and the three-dimensional compressible magnetohydrodynamic and the boundary conditions are given in Section 3. In Section 4, the numerical results are presented. Finally, the summary of this investigation is given in Section 5.

2. A brief description of the observed AR 10720 during the CME period

Active region NOAA AR 10720 first appeared near the east limb on January 10, 2005, but it was not until January 15 that this region produced several flares. GOES reported an X2.6 X-ray flare between 22:25 and 23:31 UT with peak emission at 23:02 UT. At 23:06 UT a halo coronal mass ejection was seen by LASCO/C2, shown in Fig. 1a, which showed the very bright loop front, mainly in the north-west (NW) quadrant. The event was seen in LASCO/C3 at 00:18 UT of January 16, 2005 as shown in Fig. 1b. Fig. 2a and b showed the MDI magnetogram (17:45 UT) and BBSO H-alpha (22:31 UT) at 15 January 2005. Since the MDI magnetogram only has line-of-sight (LOS) magnetic field measurements, our model needed BBSO's digital vector magnetogram (DVMG) for the study. The data we used has a cadence of ~2 min.

3. The model

The employed model is the recently developed data-driven 3D MHD model (Wu et al., 2005, 2006). This model is based on the conservation laws with higher order transport effects (i.e. magnetic diffusion, thermal conduction, viscos-

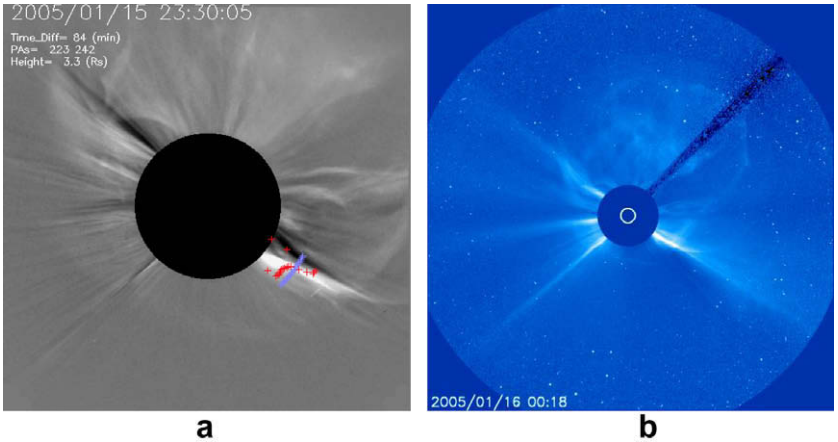

Fig. 1. Observed coronal mass ejection of January 15, 2005 by LASCO/C2 at 23:05UT (left) and January 16, 2005 by LASCO/C3 at 00:18UT (right). The red crosses and blue lines are traces of the streamer feature; it is not related to the halo CME which we have studied. (For interpretation of color mentioned in this figure legend the reader is referred to the web version of the article.)

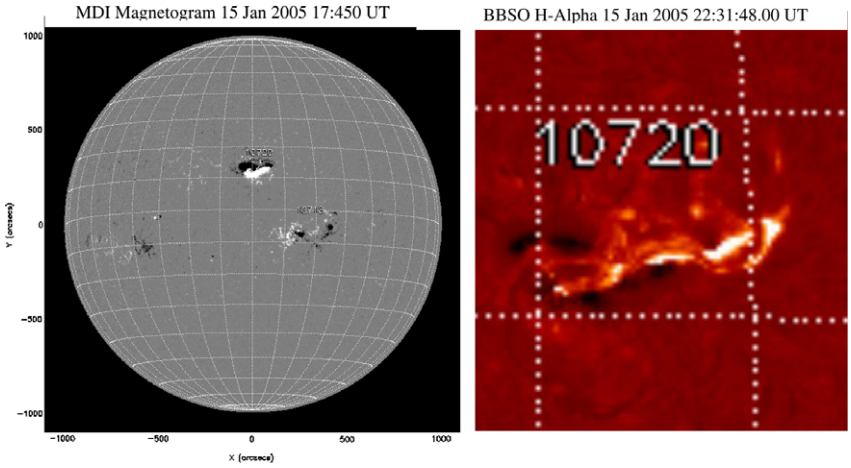

Fig. 2. Observed AR 10720 of January 15, 2005 at 17:45:00 UT from MDI (left) and BBSO H-alpha sub-field at 22:31:48 UT (right).

ity, etc.) and includes the additional forces induced by differential rotation and meridional flow. In addition, the induction equation is included to account for the dynamics effects caused by the interaction between the plasma flow and the magnetic field. These equations are given by Wu et al. (2006); we will not repeat them here. An illustration of the concept of this data driven three-dimensional compressible and resistive MHD model is depicted in Fig. 3. The computational domain is a 3D rectangular box in Cartesian coordinates with $256 \times 256 \times 101$ grids in the x, y and z directions, respectively in accordance with NOAA AR 10720 BBSO's digital vector magnetogram (DVMG) which corresponds to a spatial extend of $222 \times 222 \times 87$ Mm. The ambiguity of the transverse magnetic field has been corrected and the magnetic vector and geometric mapping of the observation in the image plane have transformed into heliograph plane (Gary and Hagyard, 1990). The lower physical boundary conditions are derived from the method of characteristics (Nakagawa, 1981a,b; Wu and Wang, 1987). From the characteristics theory, if the eigenvalue (i.e. characteristic wave speed) is negative, that means the boundary condition will be affected by the computational domain, and we have to use the compatibility equation to determine the physical parameters. The number of compatibility equations that have to be used is determined by the number of negative eigenvalues. In this study, we have $|u_z| < V_s, V_A, V_f$, therefore $u_z, u_z - V_s, u_z - V_A$, and $u_z - V_f$ are negative at the photosphere. Furthermore note that u_z is a set of two degenerated eigenvalues of the normal characteristic equations. Hence, these five parameters determined by five compatibility equations, and the three remaining physical

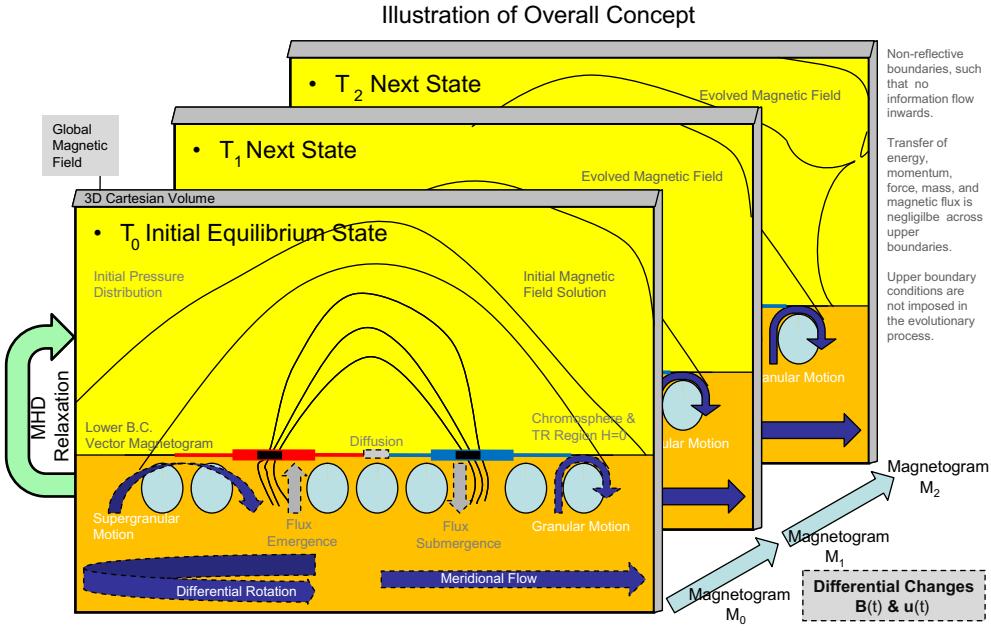

Fig. 3. Illustration of overall concept of a three-dimensional data-driven, compressible resistive MHD simulation model for active region evolution.

parameters are to be given explicitly. In this study, the three given parameters that drive the model are the three components of the magnetic field, given by disjunct time series of photospheric vector magnetogram. $u_z - V_f$, $u_z - V_s, u_z - V_A, u_z|u_z| \leq V_A, V_s, V_f$ The detailed derived expressions which describe these time-varying physical parameters, p, ρ, $\vec{B}$, and $\vec{u}$ (the pressure, density, magnetic field, and velocity field, respectively) on the lower boundary obtained from the method of characteristics are given in the appendix of Wu et al. (2006). The boundary conditions used for the four sides and top boundary are non-reflective boundary. There are two steps to implement these calculations: (i) use the observed line-of-sight magnetic field component of AR 10720 from BBSO's DVMG (Spirock et al., 2001) to construct a three-dimensional potential field model in the computation volume, as the initial trial condition. At the lower boundary the measured three components of magnetic field are given without change during the course of this simulation. (ii) Since there are no density measurements available from the photosphere we simply assume that the "initial" trail density distribution at the photospheric level is directly proportional to the value of the magnitude of the transverse field and then decreases exponentially with the scale height. These trial conditions are to initiate the numerical computation. Then, the plasma and field will evolve to a new magnetohydrodynamic equilibrium state which should be able to represent the solar atmosphere conditions at a specific time. When we input another set of observed data following the same procedure, we will obtain another magnetohydrodynamic state at another time. Thus, within the computational domain, the continuous time evolution of the solar atmosphere 8 physical parameters are obtained. These results are presented in the next section.

4. Results

By inputs of the measured three components of magnetic field of AR 10720 together with assumed density distribution as pointed out in the previous section, we obtained the four major non-potentiality parameters, following Falconer et al. (2002), shown in Fig. 4 during the period of 22:10–23:50 UT, January 15, 2005. These non-potentiality parameters are (i) the length of strong magnetic shear (>45°) and the strong transverse field (>300 gauss) of the main neutral line, (ii) the total magnetic flux content (Φ), (iii) the net electric current (I_N), and (iv) the flux normalized of the field twist ($\alpha = \frac{\mu I_N}{\Phi}$). The horizontal bold line indicates the impulsive phase of a flare (which is not discussed here). The solid vertical line indicates the CME appearance in the LASCO/C2 field of view and the vertical dashed line indicates the back extrapolated time of the CME launch. One of the general characteristics we have recognized is that before the CME, all these four parameters are increased in the build-up phase and they decline after the CME as expected. It is worth noting that Schrijver et al. (2005) have suggested that the currents associated with coronal non-potentiality have a characteristic growth and decay time scale of ~10 to 30 h. In our calculation we only simulate the rise and decay phases of non-potentiality around the CME. Now, we will examine the surface features. Fig. 5 shows the evolution of magnetic shear (L_{SS}) from 22:33–23:15 UT, and we again observe the increase of the magnetic shear before the CME, and then the decrease after the CME. It is worth noting that the fragmentation of magnetic shear at the north-west quadrant does not appear at the north-east quadrant. This feature indicates the increase of a magnetic shear is rather homogeneous at the north-east quadrant. On the other hand, the fragmentation at the north-west quadrant represents the severe inhomogenity where it could be the source of the instability to trigger a CME. This can be understood from the MHD instability theory in which the highly non-uniform twist will induce the kink instability (Lapenta et al., 2006, Biskamp, 1993). However, we have not examined this topic in detail here. It is our intent to investigate it later. At time of 23:15 UT, the magnetic shear at the north-west quadrant has almost disappeared and the CME has already launched. By looking at the north-east quadrant, the magnetic shear has shown little change which is why we suggest that, even though there is a strong shear with homogenous strength, it could be stable for a long time without eruption. Thus, strong magnetic shear is a necessary condition, but not sufficient to produce eruption. In the next few figures we show some other physical properties

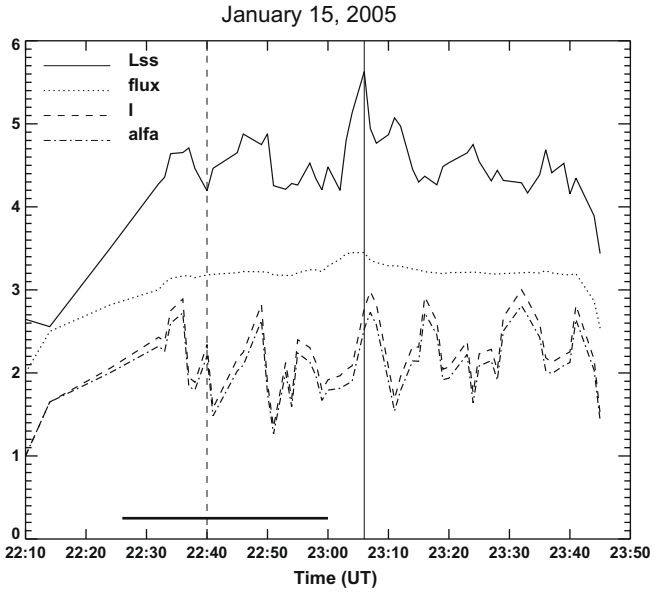

Fig. 4. The simulated non-potential parameters (i.e. L_{ss}, length of magnetic shear of the main neutral line (in units of 2×10^4 km); magnetic flux (Φ) (in units of 5×10^{21} Mx); net electric current (I_N) (in units of 3×10^{11} A); and normalized measure of the field twist (α) (in units of 1.5×10^{-5} km)) at various times for AR 10720, on January 15, 2005. The horizontal bold line indicates the impulsive phase of a flare (onset-to-maximum of the soft X-ray emission), the vertical solid line shows the occurrence of a CME in the LASCO/C2 field of view, and the vertical dashed line indicates the back extrapolated time of the CME launch.

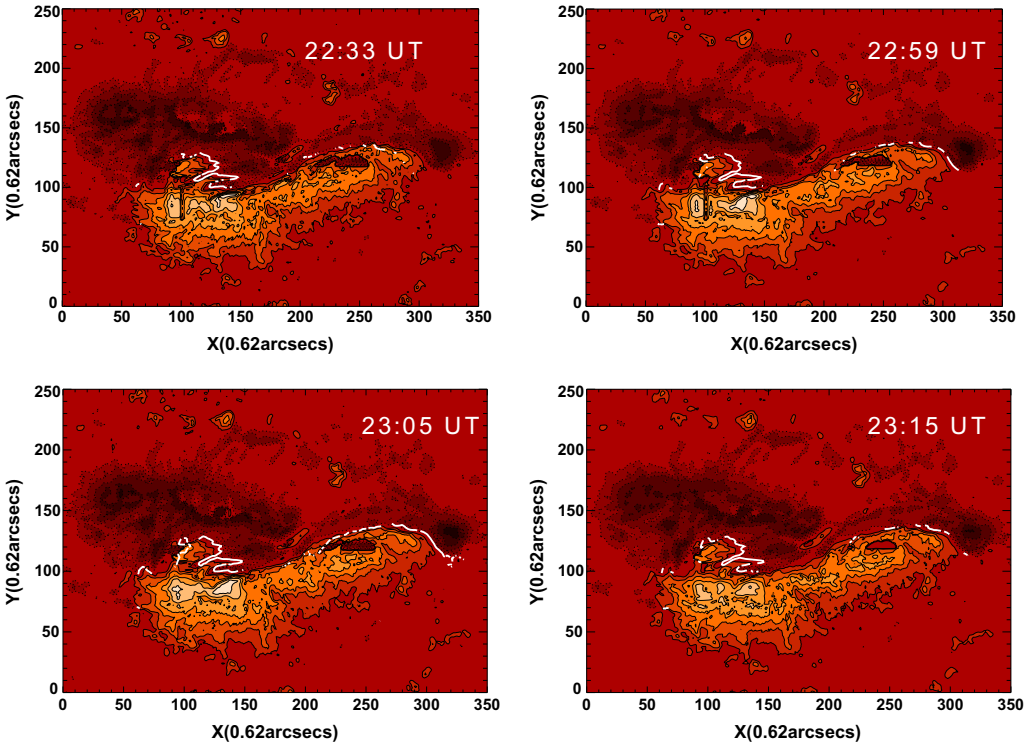

Fig. 5. The simulated evolution of the length of magnetic shear of the main neutral line (L_{ss}) of AR 10720 during the period 22:33−23:15 UT on January 15, 2005. The contours of the line-of-sight magnetic field (B_z) with the solid lines and broken lines representing the positive and negative polarity, respectively. The color scale indicates the strength of the line-of-sight magnetic field ($-2400\ \mathrm{G} \leqslant B_z \leqslant 1700\ \mathrm{G}$) contours in which the bright color represents the positive field, and the dark color represents the negative field. (For interpretation of color mentioned in this figure legend the reader is referred to the web version of the article.)

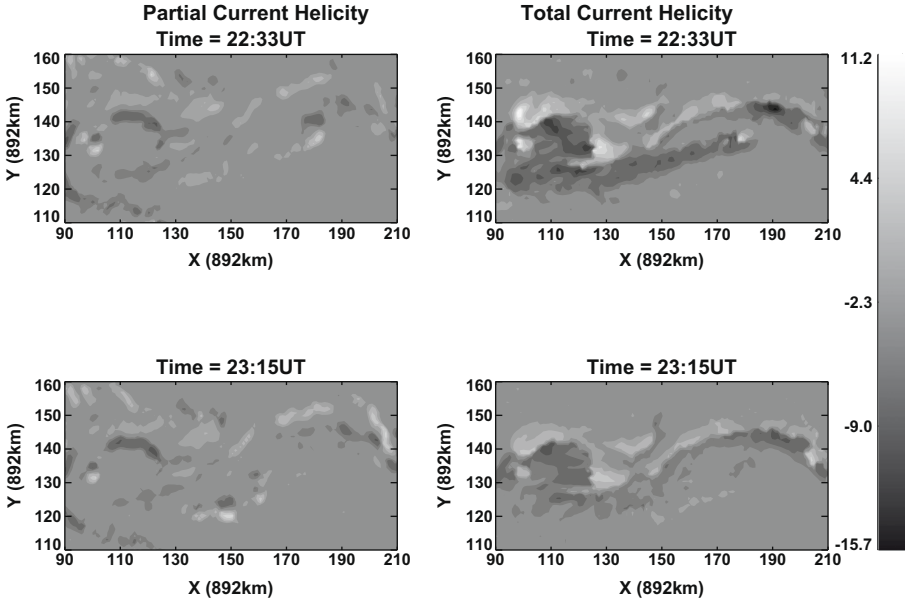

Fig. 6. The simulated partial (left) and total (right) current helicity, respectively. The magnitude is indicated by the code bar on the right which is in the range of −15.7 to +11.2 (10^{-3} G^2/m).

during that same period of time (22:33–23:15 UT); Fig. 6 shows the variations of the partial (right) and total (left) current helicity before (22:33 UT) and after (23:15 UT) of a CME. The total current helicity is given by:

$$H_c = \vec{B}\cdot\vec{J} = \vec{B}\cdot(\nabla\times\vec{B}) = B_x\left(\frac{\partial B_z}{\partial y}-\frac{\partial B_y}{\partial z}\right)+B_y\left(\frac{\partial B_x}{\partial z}-\frac{\partial B_z}{\partial x}\right)+B_z\left(\frac{\partial B_y}{\partial x}-\frac{\partial B_x}{\partial y}\right) \quad (1)$$

Usually, only the partial current helicity (i.e. third term) can be obtained from a vector magnetogram, but with the aid of the MHD model we are able to compute all three terms, thus, we define it as the "total current helicity". As we can see from Eq. (1), the total current helicity includes the effects of the vertical gradient magnetic field. For both cases, it indicates that the current helicity is decreased after the CME which is consistent with those non-potentiality parameters shown in Fig. 4. It is also worth noting that differences in strength between the partial and total current helicity is about a factor of two and the distribution of the total current helicity is much more cohesive than the partial one. The amount of energy resulting from the dissipated current at the surface corresponding with the current helicity is 3×10^{32} erg which is adequate to propel a CME. It is also worth noting that the total current helicity changes are related to the local twist of the magnetic field in the photosphere, thus the increase and decrease of total current helicity corresponds to the increase and decrease of the magnetic shear as shown in Figs. 4 and 5. Another feature worth noting is that variation of current (I_N) and twist (α) are well matched spatially, which says that the net electric current is caused by the twist of the field line as shown in Fig. 4.

In order to reveal the current system of AR 10720, we have plotted the evolution of vertical and transverse current at the surface in Fig. 7 before and after the occurrence of a CME. The bright and dark regions represents the upward and downward current density where the magnitude is given by the color bar in the range between −2.0 and 2.4 kG/Mm., the arrows represent the transverse cur-

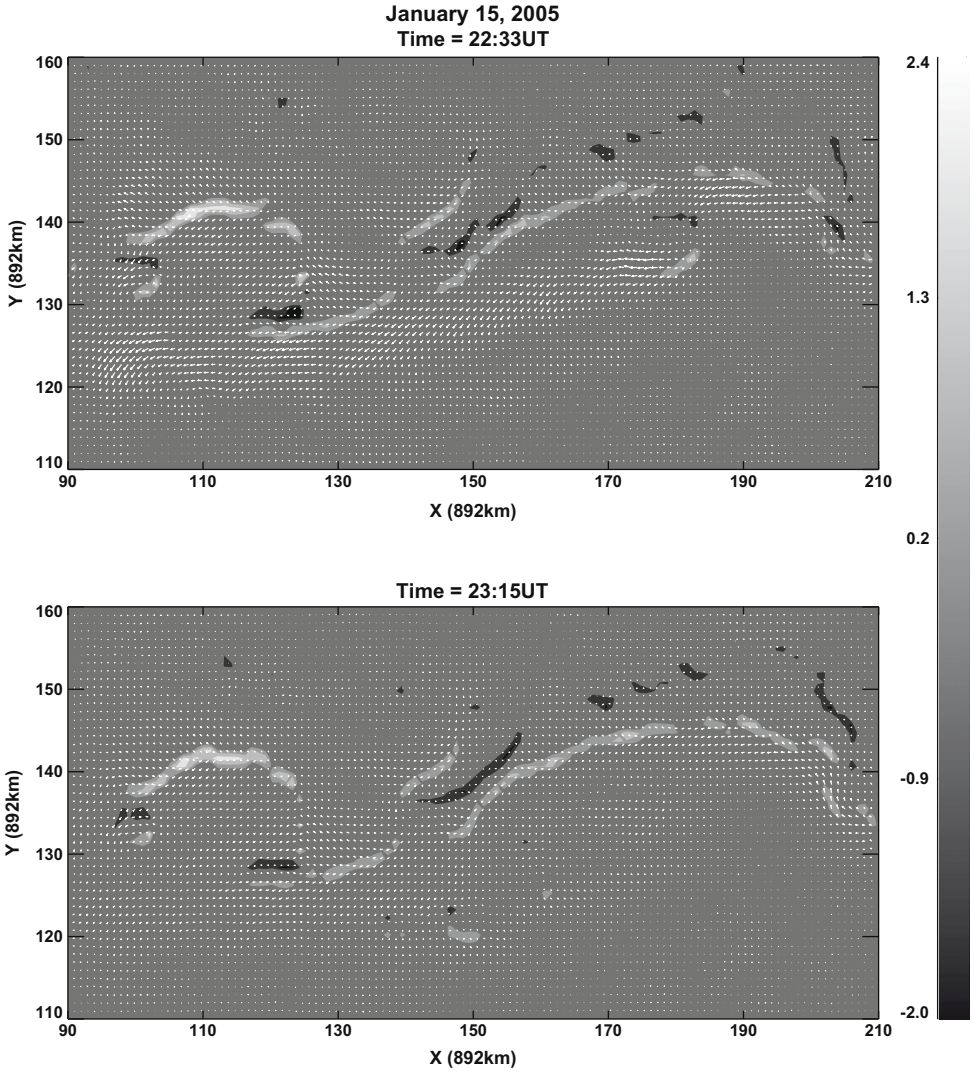

Fig. 7. The simulated vertical and transverse current for AR 10720 from 22:33–23:15 UT, on January 15, 2005, where the dark and bright thick lines represents the intensity of the upward and downward vertical current and the arrows represents the transverse current.

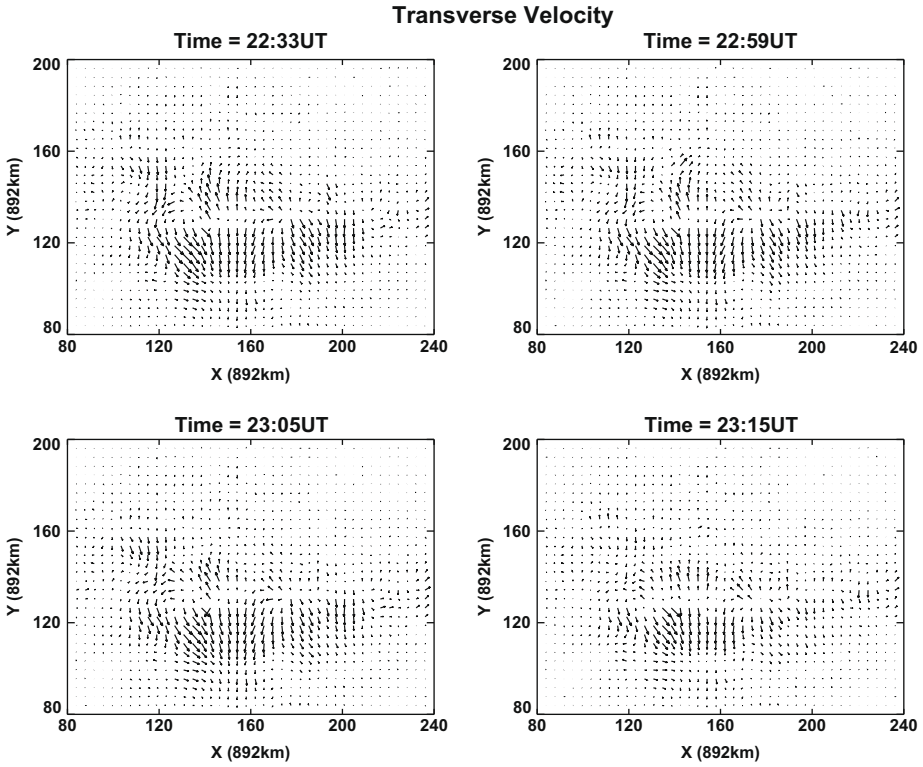

Fig. 8. The simulated transverse velocity ($-2.2\ \mathrm{km\ s^{-1}} \leqslant V_x \leqslant 3.1\ \mathrm{km\ s^{-1}}$; $-3.2\ \mathrm{km\ s^{-1}} \leqslant V_y \leqslant 3.8\ \mathrm{km\ s^{-1}}$) evolution of AR 10720 during the period 22:33–23:35 UT of January 15, 2005.

rent density where the magnitude of the current density is in the range of −0.2 to 0.76 kG/Mm. By examining these two panels further, the changes before and after the appearance of a CME are clearly indicated. For instance, the significant decreasing of transverse current density after the CME was launched at the lower part of the panel and the vertical current density changes as shown at the location of $\sim 182 \times 135$ and then completely disappears after the CME. These are all qualitative descriptions, making it difficult to arrive at a quantitative conclusion, because it is not possible to identify the exact location of the CME at the solar surface.

In Fig. 8, we show the evolution of the transverse velocity on the photosphere. Interestingly, the evolution of the transverse velocity on the photosphere can cause the variation of electric field (i.e. $\vec{E} \sim \vec{V} \times \vec{B}$), consequently this corresponds to the transverse currents shown in Fig. 7.

5. Concluding remarks

In this paper, we have used a three-dimensional, time-dependent, compressible magnetohydrodynamic (MHD) model together with photospheric vector magnetic field measurements to investigate the transport and change of the current helicity and magnetic non-potentiality properties of AR 10720 before and after a CME. Usually, the current helicity is deduced from measurements that are limited to one term (i.e. the third term of Eq. (1)) on the basis of the line-of-sight (LOS) component of the magnetic field and horizontal gradient of the transverse field. However, the total current helicity can be obtained self-consistently with the aid of an MHD model with dynamical effects (i.e. the interaction between magnetic field and plasma) (see Eq. (1)).

Specifically, our results also include the photospheric surface current system as shown in Fig. 7. To understand the physics of this surface current in relation to coronal current, we devise this current system into three parts; interior current, I_i which occurs in the interior of the Sun, a subphotosphere quantity, coronal current, I_c being σE_z and the surface (transverse) current I_s, where $I_s = (I_x^2 + I_y^2)^{1/2} = \sigma(E_x^2 + E_y^2)^{1/2}$, σ being the classical electric conductivity and E_x, E_y and E_z are the outputs of the model. Further, we define the same current component in the phase of the eruption as I_c^*, I_s^*, and I_i^*. Here I_c^* and I_i^* will not be able to be estimated due to insufficient conditions, but I_s^* can be estimated from our calculation shown in Fig. 7 such that $I_s^* = I_s + \delta I_s$, where δI_s is the induced surface current caused by the interaction between the plasma motion and magnetic field. If it is assumed that I_i remains constant since it is part of the global subsurface current system, whereas the coronal current contained in the erupting structure decreases due to inductive effects, then current conservation implies that I_s^* increases before eruption and decreases after eruption. Fig. 7 clearly shows the change of this induced surface current δI_s. Based on the present calculation, the δI_s has a value of 1.5×10^{11} A, which corresponds to 3×10^{32}

erg which is enough energy to propel this CME. This parameter could be another important non-potentiality property for forecasting purposes.

In summary, this combined modeling and data analyses study of AR 10720 has revealed some important knowledge for the understanding of active region evolution. The magnetic non-potentiality parameters and current helicity are closely related to the photospheric surface dynamo. The modeling has given us the ability to quantify these magnetic non-potential parameters. It is worth conducting more studies of this type to establish a statistical meaning of these physical parameters for potential forecasting of solar eruptive events.

Acknowledgements

The work performed by S.T.W., A.H.W. is supported by AFOSR FA9550-07-1-468, NSF ATM-0754278, and NSF AST-0132798 via AURA subaward C10596A. G.A.G. is supported by NASA NNM05AA22A. A.K. and J.R. acknowledge the Grant VEGA 2/0064/09. B.V. is grateful for the hospitality during his stay at UAHuntsville.

References

Biskamp, D., 1993. Nonlinear Magnteohydrodynamics, Cambridge University Press, p. 67.

Chae, J. Observational determination of the rate of magnetic helicity transport through the solar surface via the horizontal motion of field line footpoints. ApJ 560, L95, 2001.

Chae, J., Moon, Y.J., Park, Y.D. Determination of magnetic helicity content of solar active regions from SOHO/MDI magnetograms. Solar Phys. 223, 39, 2004.

Deng, Y.Y., Wang, J.X., Yan, Y.H., Zhang, J., 2001. Evolution of magnetic nonpotentiality in NOAA AR 9077. Solar Phys. 204, 13.

Demoulin, P., Mandrini, C.H., Van Driel-Gesztelyi, L., Thompson, B.J., Plunkett, S., Kovari, Z., Aulanier, G., Young, A. What is the source of the magnetic helicity shed by CMEs? The long-term helicity budget of AR 7978. Astron. Astrophys. 382, 650, 2002.

Falconer, D.A., Moore, R.L., Gary, G.A. Correlation of the coronal mass ejection productivity of solar active regions with measures of their global nonpotentiality from vector magnetograms: baseline results. ApJ 569, 1016, 2002.

Allen Gary, G., Hagyard, M.J. Transformation of vector magnetograms and the problems associated with the effects of perspective and the azimuthal ambiguity. Solar Phys. 126, 21, 1990.

Kusano, K., Maeshiro, T., Yokoyama, T., Sakurai, T. Impulsive variations of the magnetic helicity change rate associated with eruptive flares. ApJ 577, 501, 2002.

Lapenta, G., Furno, I., Intrator, T., Delzanno, G.L. Kink instability of flux ropes anchored at one end and free at the other. J. Geophys. Res. 111, A12506, 2006.

Liu, J.H., Zhang, H.Q. The magnetic field, horizontal motion and helicity in a fast emerging flux region which eventually forms a delta spot. Solar Phys. 234, 21, 2006.

Liu, J.H., Zhang, H.Q. The relationship between inductive electric field and flares. Adv. Space Res. 39, 1835, 2007.

Moon, Y.J., Chae, J., Wang, H., Choe, G.S., Park, Y.D. Impulsive variations of the magnetic helicity change rate associated with eruptive flares. ApJ 580, 528, 2002.

Nindos, A., Zhang, J., Zang, H.Q. The magnetic helicity budget of solar active region and coronal mass ejections. Astrophys. J. 594, 1033, 2003.

Nindos, A., Andrews, M.D. The association of big flares and CMEs: what is the role of magnetic density. ApJ 616, L175, 2004.

Nakagawa, Y. Evolution of magnetic field and atmosphere response I. Three-dimensional formulation by the method of projected characteristics. ApJ 247, 707, 1981a.

Nakagawa, Y. Evolution of magnetic field and atmospheric response II. formulation of proper boundary equations. ApJ 247, 719, 1981b.

Schrijver, A., Carlous, J., DeRosa, A., Marc, L., Title, A., Alan, M., Metalf, A., Thomas, R. The nonpotentiality of active region coronae and the dynamics of the photospheric magnetic field. ApJ 628, 501, 2005.

Spirock, T., Denker, C., Chen, H., Chae, J., Varsik, J. Wang. H., Goode, P.R., Marquette, W., 2001. Advanced solar polarimetry theory, observation and instrumentation. In: Sigwath M. (Ed.), 20th NSO/SAC Summer Workshop, ASP Conference Proceedings, vol. 236. Astronomical Society of the Pacific. ISBN: 1-588381-073-0, p. 65.

Wu, S.T., Wang, A.H, Falconer, D.A., 2005. A three-dimensional magnetohydrodynamic (MHD) model of active region evolution. In: Dere, K.P., Wang, J.X., Yan, Y. (Eds.), Coronal and Stellar Mass Ejections, IAU Symposium No. 226, 291.

Wu, S.T., Wang, A.H., Liu, A., Yang, A., Hoeksema, J. Todd, Data driven magnetohydrodynamic (MHD) model for active region (AR) evolution. ApJ 652, 800, 2006.

Wu, S.T., Wang, J.F. Numerical tests of a modified Full-Implicit-Continuous-Eulerian (FICE) scheme with projected normal characteristic boundary conditions for MHD flows. Comput. Methods Appl. Mech. Eng. 64, 267, 1987.